Article:
Pan, F., Aaron Lau, K.H., Messersmith, P.B. et al. (2020) Interfacial assembly inspired by marine mussels and antifouling effects of polypeptoids : a neutron reflection study. Langmuir, 36 (41). pp. 12309-12318. ISSN: 0743-7463

https://doi.org/10.1021/acs.langmuir.0c02247

LANGMUIR

pubs.acs.org/Langmuir Article

Interfacial Assembly Inspired by Marine Mussels and Antifouling Effects of Polypeptoids: A Neutron Reflection Study

Fang Pan, King Hang Aaron Lau, Phillip B. Messersmith, Jian R. Lu,* and Xiubo Zhao*

Cite This: *Langmuir* 2020, 36, 12309−12318 Read Online

ACCESS | Metrics & More | Article Recommendations | Supporting Information

ABSTRACT: Polypeptoid-coated surfaces and many surface-grafted hydrophilic polymer brushes have been proven efficient in antifouling-the prevention of nonspecific biomolecular adsorption and cell attachment. Protein adsorption, in particular, is known to mediate subsequent cell-surface interactions. However, the detailed antifouling mechanism of polypeptoid and other polymer brush coatings at the molecular level is not well understood. Moreover, most adsorption studies focus only on measuring a single adsorbed mass value, and few techniques are capable of characterizing the hydrated *in situ* layer structure of either the antifouling coating or adsorbed proteins. In this study, interfacial assembly of polypeptoid brushes with different chain lengths has been investigated *in situ* using neutron reflection (NR). Consistent with past simulation results, NR revealed a common two-step structure for grafted polypeptoids consisting of a dense inner region that included a mussel adhesive-inspired oligopeptide for grafting polypeptoid chains and a highly hydrated upper region with very low polymer density (molecular brush). Protein adsorption was studied with human serum albumin (HSA) and fibrinogen (FIB), two common serum proteins of different sizes but similar isoelectric points (IEPs). In contrast to controls, we observed higher resistance by grafted polypeptoid against adsorption of the larger FIB, especially for longer chain lengths. Changing the pH to close to the IEPs of the proteins, which generally promotes adsorption, also did not significantly affect the antifouling effect against FIB, which was corroborated by atomic force microscopy imaging. Moreover, NR enabled characterization of the *in situ* hydrated layer structures of the polypeptoids together with proteins adsorbed under selected conditions. While adsorption on bare SiO_2 controls resulted in surface-induced protein denaturation, this was not observed on polypeptoids. Our current results therefore highlight the detailed *in situ* view that NR may provide for characterizing protein adsorption on polymer brushes as well as the excellent antifouling behavior of polypeptoids.

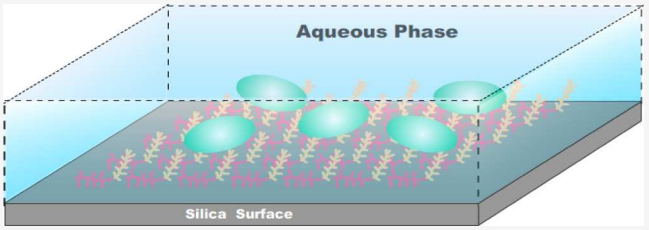

INTRODUCTION

Protein adsorption onto solid substrates is a widespread phenomenon, and its prevention is critical for proper functioning of medical devices and implants, as well as in bioseparation and other applications involving surfaces prone to contamination.[1−6] The adsorption of proteins in these cases is largely of a nonspecific nature, and there is little control over the structure and composition of the adsorbed protein layer. When proteins from blood are adsorbed onto the surfaces of medical implants, the interfacial processes could undermine device integration at an early stage, trigger adverse cellular responses, and compromise the device's performance and fate. In the use of porous media (e.g., porous filtration membranes or packed columns), protein-surface interactions form an important basis for separation and purification and even the tuning of refoldable 3D structures. However, irreversibly adsorbed proteins not only reduce the flux but also pose the risk of cross-contamination. Therefore, techniques or materials that can effectively inhibit nonspecific protein adsorption have a variety of applications.

A number of factors affect the extent of protein adsorption or protein-substrate interactions.[4,6−12] These include protein size, shape, stability, charge and charge distribution, concentration, pH, and ionic strength. Surface properties of the substrate material such as its chemical nature, hydrophobicity, charge, and charge density also play important roles. Electrostatic and hydrophobic interactions are major driving forces of protein adsorption on hydrophilic and hydrophobic surfaces, respectively.[13] High protein adsorption generally occurs on hydrophobic surfaces. On the other hand, a range of strategies related to surface wetting/hydrophobicity have been explored to minimize adsorption, including air-trapping superhydrophobic surfaces as well as highly hydrated zwitterionic surfaces.[1,6] Once adsorbed, further interactions between protein molecules and the interface, including dissociation and re-association of hydrogen bonding and

Received: July 30, 2020
Revised: September 24, 2020
Published: September 24, 2020

https://dx.doi.org/10.1021/acs.langmuir.0c02247
Langmuir 2020, 36, 12309−12318

other intermolecular interactions, may result in protein structural deformation and possible unfolding.

Antifouling polymer brushes have been a main approach developed to reduce protein adsorption.[3,5,6,14] Polymers such as poly(vinyl chloride), poly(ethylene oxide), poly(etherurethane), poly(dimethylsiloxane), poly(*N*-isopropylacrylamide), and poly(tetrafluoroethylene) and their copolymers can provide different extents of protein resistance, but their hemo-compatibility is often poor.[3,15] Poly(ethylene glycol) (PEG) and related graft co-polymers have also been widely reported, although in some cases they may encounter chemical or enzymatic degradation.[16] In our previous studies, we have demonstrated that coatings with zwitterionic phosphorylcholine (PC) containing copolymers can substantially reduce protein adsorption.[3,4] We also reported antifouling brushes composed of peptoids, which mimic the polypeptide backbone.[17−19] However, overall, neither the solid-liquid interfacial structure of peptoid and other polymer brushes nor the physical state of residual proteins subsequently adsorbed has been well studied. Furthermore, most studies focus on short-term experiments demonstrating "zero" adsorption of novel systems, but fouling and subsequent protein-mediated interactions, nonetheless, occur in practical settings, not least around defects sites and as antifouling layers degrade over time.[6]

In this work, we report recent studies of *in situ* neutron reflection (NR) dedicated to improving this part of understanding. Specular NR is capable of quantitative determination of the thickness and uniformity of an interfacial layer with subnanometer sensitivity along the surface normal direction.[7,9,11,20−24] It effectively determines how the volume fraction (ϕ) of the layer varies with the distance perpendicular to the interface. The technique has been widely used in determining the interfacial layer structure of a variety of soft matters such as surfactants,[25−30] peptides,[21,22,25,26,31,32] proteins,[33−37] antibodies,[2,38−43] DNAs,[44,45] polymers,[44] and lipids.[36,46] As an example system, we employed a set of peptoid peptidomimetic polymers (PMPs) that we have previously demonstrated to prevent protein adsorption and cell attachment above certain chain length-dependent critical grafted chain densities.[16,18,47] PMPs form an excellent model brush system because of their exact chain lengths controlled by solid phase synthesis.[18,48]

From optical matrix analysis of NR reflectivity profiles, we were able to obtain polymer density height-profiles of grafted PMP layers. Focusing on intermediate PMP-grafted densities that allowed some protein adsorption, we likewise obtained adsorbed layer profiles of two model proteins with a similar isoelectric point (IEP)-human serum albumin (HSA, 67 kDa; IEP = 4.8) and the much larger fibrinogen (FIB, 340 kDa; IEP = 4.3). The NR technique enabled *in situ* measurements of proteins interacting with the underlying brush in a hydrated state, simulating native biological environments. We were therefore able to characterize the heterogeneous brush and adsorbed protein layer profiles that depended on both the protein, the experimental pH, as well as on the brush chain length, thus informing the future design of antifouling polymer brushes.

RESULTS AND DISCUSSION

In this work, NR has been used to investigate protein adsorption on grafted PMPs at the solid-liquid interface, with the substrate being the SiO_2 surface on a silicon crystal block and the solution being aqueous buffer containing the peptoid or protein (see the Supporting Information for NR chamber configuration). The PMP is a previously reported design containing two parts (Figure 1): a mussel adhesive-inspired

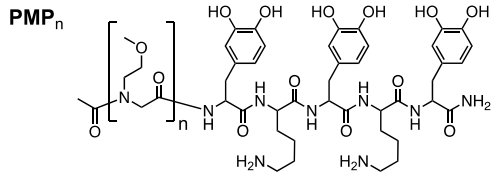

Figure 1. Chemical structure of PMPs (PMP_n) where n = 15, 20, 30, and 50, with an antifouling polypeptoid segment and DOPA-Lys-DOPA-Lys-DOPA pentapeptide surface adhesion unit.

pentapeptide (DOPA-Lys-DOPA-Lys-DOPA) and a peptoid antifouling chain.[17] The short DOPA pentapeptide provides robust adhesion of the coupled peptoid chain to wet surfaces. DOPA has been used to couple a variety of molecules on diverse substrates without affecting the functionality of the immobilized molecule.[49] Therefore, we believe that DOPA will simply serve to immobilize PMP and not interfere with antifouling properties.

The chosen peptoid homopolymer ("polypeptoid") has methoxyethyl side chains resembling the repeating unit of PEG.[17,47] We have previously shown that this overall PMP design is able to prevent protein adsorption as well as fibroblast and bacterial cell attachment above certain "critical" surface-grafted chain densities that range from 0.4 to 0.8 chain/nm^2 as the chain length decreases from 50 to 15 repeating units.[16−18,47] In this study, we focus on lower chain densities. This allowed us to observe some limited protein adsorption in order to facilitate investigation of the effects of chain length, protein size, and buffer pH, all of which are major variables controlling protein interactions with a polymer brush. We have previously used such a methodology to study differences in electrostatic interactions of various zwitterionic antifouling peptoid designs.[18] These subcritical densities also mimic situations inevitably encountered in practical applications, such as defect sites and long-term degradation of polymer brush surfaces.[6]

PMP Grafting Analysis. Typical NR data for grafting of polypeptoids 15, 20, 30, and 50-mer long are shown in Figure 2. Grafting of polypeptoids was evident from the deviation of reflectivity profiles from the reference measured at the bare SiO_2/D_2O interface control (Figure 2A). Reflectivity profiles were analyzed using the widely adopted optical matrix approach.[50] Analysis was pursued by first calculating a reflectivity profile based on an assumed interfacial structure and then comparing it with the measured one. The process was iterated until an acceptable fit was obtained within the experimentally sensitive Q range of 0.012−0.25 Å^{-1}. The parameters obtained from optical matrix data analysis are listed in Table 1, and the molecular weights and the scattering length densities (SLDs) obtained from NR fitting are summarized in Table S1.

The fitting to the bare SiO_2/D_2O interface led to the native oxide layer thickness of 13 Å and its SLD of 3.4×10^{-6} Å^{-2}. Because the SLD for this layer was the same as commonly accepted values of solid bulk SiO_2, the result indicated a void-free and smooth SiO_2 substrate surface. Subsequent analysis of polypeptoid grafting was undertaken by assuming that the

https://dx.doi.org/10.1021/acs.langmuir.0c02247
Langmuir 2020, 36, 12309−12318

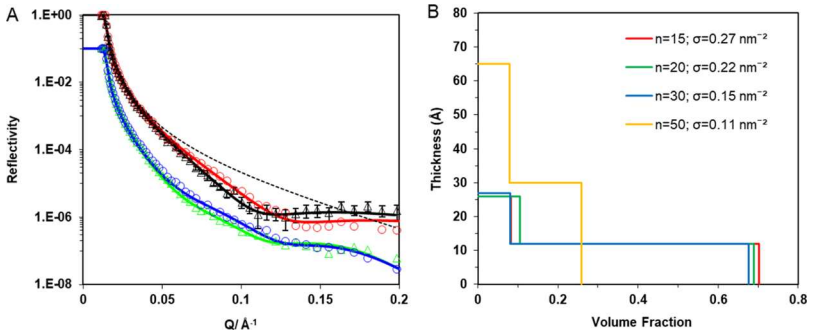

Figure 2. (A) Representative plots of NR profiles of PMPs at the interface of the SiO_2 surface and D_2O buffer (20 mM phosphate, pH 7). Data after 1 h immersion of PMP_{15} (black and red) and PMP_{50} solutions (green and blue), both at 0.1 mM before (△) and after buffer wash (○) are shown. The solid lines are the best fits to the measured data. The dashed line is the bare SiO_2/D_2O reference. For clarity, PMP_{50} data have been shifted down 1 order of magnitude along the vertical axis, and error bars are only shown in one set of data. The thickness of SiO_2 was found to be 13 ± 1 Å. Parameters obtained by the data fitting are shown in Table 1. (B) Two-step polymer volume density plots as a function of height from the SiO_2 surface measured for PMP_n (n = 15, 20, 30, and 50). The corresponding chain densities (σ) are shown in the legend.

Table 1. Best Fit Parameters from the Experimental Data Shown in Figure 2A

samples/conc	$\tau \pm 1$ (Å)	$(\rho \pm 0.05) \times 10^{-6}$ (Å^{-2})	φ_p	A (Å^2)	Γ (mg m^{-2})	σ (nm^{-2})
PMP_{15}/0.1 mM	16	3.4	0.702	284	1.51	0.35
	18	6.0	0.083			
PMP_{15}/0.1 mM buffer wash	12	3.4	0.702	377	1.14	0.27
	14	6.0	0.083			
PMP_{20}/0.1 mM	13	3.4	0.689	416	1.26	0.24
	18	5.9	0.105			
PMP_{20}/0.1 mM buffer wash	12	3.4	0.689	463	1.13	0.22
	14	5.9	0.105			
PMP_{30}/0.1 mM	15	3.2	0.719	522	1.37	0.19
	16	6.0	0.080			
PMP_{30}/0.1 mM buffer wash	12	3.4	0.674	679	1.05	0.15
	15	6.0	0.080			
PMP_{50}/0.1 mM	30	5.0	0.303	835	1.32	0.12
	35	6.0	0.079			
PMP_{50}/0.1 mM buffer wash	30	5.2	0.258	942	1.17	0.11
	35	6.0	0.079			

structure of the SiO_2 layer remained unchanged during the course of the experiments.

Grafting of PMP_n (n = 15, 20, 30, and 50) was undertaken by flowing polypeptoid solutions through the NR sample chamber over the SiO_2 substrate. The attached amount of PMP did not vary much against concentration within the concentration range studied (from 0.03 to 0.3 mM, after 1 h immersion). The results shown in Figure 2 and throughout this report are all based on brushes obtained at 0.1 mM.

Data analysis revealed that the distribution of grafted PMP chains of all chain lengths can be fitted to a common two-step model differing in polymer density (Figure 2B). The inner slice close to the SiO_2 surface had thicknesses (τ) of 16−30 Å with corresponding SLD of 3.4-5.2 × 10^{-6} Å^{-2}, while the second upper slice had thicknesses of 18−35 Å and SLD of 6 × 10^{-6} Å^{-2}. The large difference in SLD is indicative of the different amount of polypeptoid chains in each slice (discussed further below). The two-step model is an approximation, limited by the amount of information obtainable from NR, of the smoothly increasing density of polymer chains toward the substrate surface, as anticipated by both theoretical[47] and simulation studies.[51]

The volume fraction (ϕ) of polypeptoid in each slice, the area per molecule (A in Å^2), and the surface adsorbed amount (Γ, in mg m^{-2}) can be calculated from the following equations[9,11,21]

$$\phi_p = \frac{\rho - \rho_w}{\rho_p - \rho_w} \quad (1)$$

where ρ, ρ_p, and ρ_w are the SLDs for the slice/layer, polypeptoid, and water, respectively. The labile hydrogens in the polypeptoids were assumed to be fully exchangeable with the D_2O solvent. The equivalent area per molecule of each overall layer can be expressed as

$$A = \frac{V_p}{\tau \phi_p} \quad (2)$$

where V_p is the volume of the polypeptoid and τ is the thickness of the layer. The surface chain density (σ) is simply the inverse of A. The surface adsorbed amount (Γ) can be obtained from

$$\Gamma = \frac{MW}{6.02A} \quad (3)$$

where MW is the molecular weight of the polypeptoid (Table S1). Note that the total surface adsorbed amount could be obtained from adding the contributions from each slice from

https://dx.doi.org/10.1021/acs.langmuir.0c02247
Langmuir 2020, 36, 12309−12318

which a nominal area per molecule for the entire layer can be worked out from eq 3.

The nature of the NR experiment suited our goal of obtaining intermediate surface chain densities (σ). For example, we obtained σ = 0.27 nm^{-2} for PMP_{15} binding on SiO_2 at room temperature, compared to 0.68 nm^{-2} on a TiO_2 surface under near cloud point/lower critical solution temperature conditions (50 °C).[47] Lower grafted densities are generally obtained when grafting longer chains, and we obtained σ = 0.22, 0.15, and 0.11 chain nm^{-2} for PMP_{20}, PMP_{30}, and PMP_{50}, respectively (Figure 2B).

By comparing (Table 1) the amounts of polypeptoid bound to the surface before and after replacing the PMP solution with buffer (i.e., rinsing), we could gauge the strength of the DOPA pentapeptide for grafting polypeptoid chains. For the shortest PMP_{15} before buffer rinsing, the total thickness of the two-step layer was 36 Å, and A = 284 Å^2 and Γ_{PMP} = 1.51 mg m^{-2}. After rinsing, the total thickness was reduced to 28 Å, and A = 377 Å^2 and Γ_{PMP} = 1.14 mg m^{-2} (i.e., ca. 75% retention). For the longer polypeptoids, much higher PMP retentions were observed after rinsing, for example, for PMP_{50}, Γ_{PMP} decreased from 1.32 to 1.17 nm^{-2} (i.e., ca. 90% retention), while A increased slightly from 835 to 942 Å^2, and the total layer thickness remained at 65 Å. These results showed that PMP grafting was stronger and predominantly irreversible when each DOPA pentapeptide (together with its polypeptoid) had more space to interact with the SiO_2 surface.

The two-step interfacial structures after rinsing found for PMP_{20} and PMP_{30} were similar to PMP_{15}, with essentially the same polymer density/volume fraction in each slice. $\phi_{PMP\text{-}lower}$ was consistently around 0.7, and $\phi_{PMP\text{-}upper}$ was around 0.1 (Figure 2B). While the overall layer thickness remained ca. 26 Å and volume fraction stayed constant, the fact that the chain length was increasing contributed to the decreasing grafted chain density (Table 1). With a further increase in the chain length to PMP_{50}, the overall brush layer became thicker, and the lower chain density measured had to be matched by corresponding decreases in ϕ_p, presumably due to the steric effect of the long chain. Overall, these differences demonstrate the extension of PMP chains in a brush, consistent with past ellipsometry measurements and molecular theory.[16,47] On the other hand, the current NR studies provide better depth resolution and can therefore provide more consistent structural details about changes in the shape of the layer distribution along the surface normal and the total adsorbed amount.

For comparison, binding of the DOPA pentapeptide alone as a function of concentration has also been examined, with the results shown in Figure 3 and the best fit parameters listed in Table 2. At the 0.1 mM concentration used for PMP grafting, the surface bound pentapeptide layer could be described as a single uniform slab of 10 Å, with $\phi_{peptide}$ = 0.776 and Γ = 1.19 mg m^{-2}, respectively. These parameters match very well with those of the lower slice of PMPs, especially for PMP_{15} to PMP_{30} (Figure 2B). This supports the two-step PMP model discussed above for which the high polymer density of the inner slice consisted mostly of the DOPA pentapeptide and the low-density outer slice consisted of polypeptoids extending away from the surface, as would be expected of a surface-grafted brush. The value of $\phi_{peptide}$ and the thickness of the anchoring slice are also consistent with our earlier simulation results.[47]

At a high DOPA pentapeptide concentration of 1 mM, the peptide formed a two-step distribution with thicknesses around 10 Å each and a high total adsorbed amount of 2.7 mg m^{-2}. The inner slice was more densely packed ($\phi_{peptide}$ = 0.941) than the single layer obtained from the 0.1 mM solution above. In contrast, the outer slice was about half packed ($\phi_{peptide}$ = 0.446), indicating that some residues were "sticking up" as there was insufficient space to pack the large amount of pentapeptides available. Reduction of the pentapeptide concentration to 0.01 mM resulted in a layer thickness of only 7 Å and Γ = 0.83 mg m^{-2}. Interestingly, however, $\phi_{peptide}$ remained at 0.776, the same as for binding from 0.1 mM. Overall, given the relatively small three-fold difference in Γ as the concentration changed 100-fold from 1 to 0.01 mM, the propensity for the DOPA pentapeptide binding on SiO_2 was strong.

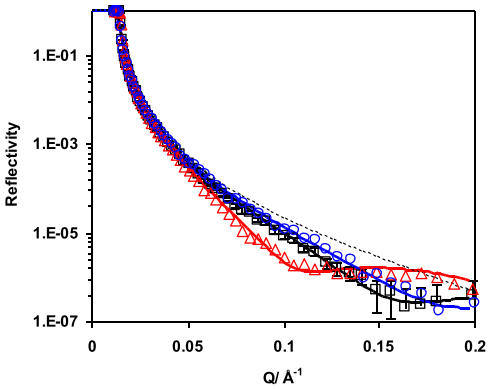

Figure 3. NR profiles at the SiO_2/D_2O buffer interface with DOPA-Lys-DOPA-Lys-DOPA at the concentration of 1 mM (△, red), 0.1 mM (□, black), and 0.01 mM (○, blue) (20 mM phosphate buffer in D_2O, pH 7). The solid lines are the best fits to the measured data. Error bars are only shown for one set of data for clarity. The NR profile at the bare SiO_2/D_2O interface is shown as reference (dashed line) with the oxide layer thickness of 13 ± 1 Å. Parameters obtained from data fitting are shown in Table 2.

Protein Adsorption on Bare SiO_2. HSA and FIB were used as model proteins to examine the antifouling effects of the polypeptoid brush surfaces. HSA is widely used in such studies and is a 67 kDa globular protein. Its longest length is around 80 Å, and its shortest length is around 45 Å.[52] Because it comprises several different domains and has large structural flexibility, it tends to deform rather easily upon interfacial adsorption.[20] HSA has an IEP of around 4.8, and its concentration in plasma is about 50 g L^{-1}. Human plasma FIB has a concentration of 1.5 to 4.0 g L^{-1} in human plasma, and it polymerizes to form fibrin during blood coagulation. It is significantly larger with a molecular weight of about 340 kDa and has dimensions ca. 470 × 50 × 50 Å^3.[53] Its IEP is around 4.3, close to that of HSA. The similarity in IEP, which specifies the protein's net charge at a given pH, and hence the long range (ca. >10 nm) of electrostatic intermolecular interactions, is the main reason for choosing HSA and FIB, even though FIB is glycosylated which would also affect its absorption behavior.

As controls, the adsorption of HSA and FIB at the bare SiO_2/D_2O buffer interface has been examined and the data are shown in Figure S1, with the best fit parameters listed in Table S2. The adsorption of HSA at the concentration of 1 g L^{-1} and pH 7 resulted in a single-layer structure at the interface. The thickness, volume fraction (ϕ_{HSA}), area per molecule (A), and surface adsorbed amount (Γ_{HSA}) were found to be 30 Å, 0.276, 9600 Å^2, and 1.15 mg m^{-2}, respectively.

https://dx.doi.org/10.1021/acs.langmuir.0c02247
Langmuir 2020, 36, 12309−12318

Table 2. Best Fit Parameters for DOPA-Lys-DOPA-Lys-DOPA Obtained from Analysis of the Reflectivity Profiles Shown in Figure 3

concentration	$\tau \pm 1$ (Å)	$(\rho \pm 0.05) \times 10^{-6}$ (Å^{-2})	φ_p	A (Å^2)	Γ (mg m^{-2})
1 mM	14	3.5	0.941	53.3	2.70
	10	5.0	0.446		
0.1 mM	10	4.0	0.776	121	1.19
0.01 mM	7	4.0	0.776	173	0.83

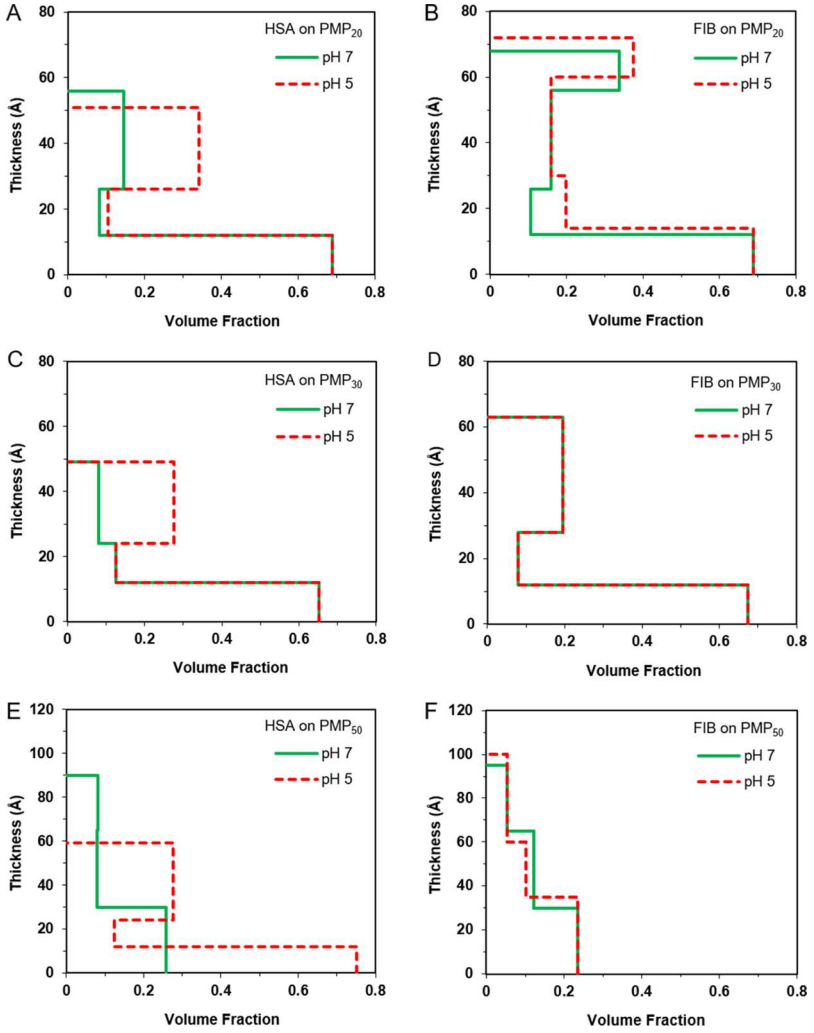

Figure 4. Layer thicknesses plots against material volume fraction after 1 h incubation in protein solutions at pH 7 (green) and pH 5 (red). Data for PMP_{20} (A,B), PMP_{30} (C,D) and PMP_{50} interfaces (E,F) are sorted by rows. HSA experimental results are shown on the left (A,C,E) and FIB results on the right (B,D,F). The corresponding NR profiles are shown in Figure S2, and the parameters obtained by data analysis are listed in Tables S3 and S4. 1 g L^{-1} HSA and 0.15 g L^{-1} FIB in 20 mM phosphate buffered D_2O were used.

Adsorption generally increases near a protein's IEP since proteins of the same species can pack more closely on a surface as charge repulsion is eliminated.[54] Accordingly, decreasing pH to 5 resulted in an increased amount of adsorbed HSA (IEP = 4.8) that has a mass distribution best fit with a two-step model of 60 Å thickness. Each modeled slice was 30 Å, with the inner surface slice having a higher $\phi_{HSA\text{-}inner}$ of 0.503 and the outer slice having only $\phi_{HSA\text{-}outer}$ = 0.179. This height distribution is consistent with HSA molecules spreading on the SiO_2 surface, presumably to increase total protein−surface interactions (i.e., surface-induced denaturation). The surface coverage (equivalent to $\phi_{HSA\text{-}inner}$) is also close to the maximum possible for random adsorption (i.e., "jamming limit" = 0.547 for roughly globular proteins).[55] Correspondingly, the total Γ_{HSA} increased from 1.15 mg m^{-2} at pH 7 to 2.84 mg m^{-2} at pH 5. These structural features are consistent with previous studies.[10,11,20]

In parallel, FIB adsorption from a solution of 0.15 g L^{-1} at pH 7 has also been examined. A two-step model indicating protein spreading was already required to fit the data for this larger protein far above its IEP of 4.3. Similar to HSA, the total thickness was found to be 60 Å and each slice was again 30 Å thick, with the inner slice being denser ($\phi_{FIB\text{-}inner}$ and $\phi_{FIB\text{-}outer}$ were 0.374 and 0.125, respectively). The total adsorption (Γ_{FIB}) was 2.4 mg m^{-2}.

Protein Adsorption on PMPs. Further experiments were carried out to investigate the antifouling properties of the PMP brush surfaces. The intermediate grafting densities grafted (Table 1) are at roughly half the critical densities[18,47] required

https://dx.doi.org/10.1021/acs.langmuir.0c02247
Langmuir 2020, 36, 12309−12318

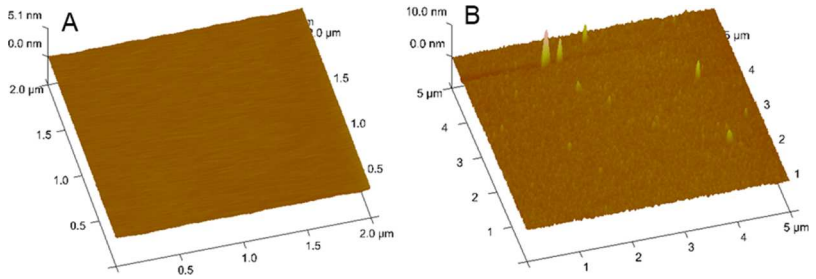

Figure 5. AFM images of PMP_{30} (0.1 mM and pH 7) grafted on silica substrates (A) and followed by FIB (0.15 g L^{-1}, pH 5) adsorption (B).

to essentially eliminate adsorption. This enabled measurable protein adsorption in order to study the effects of chain length, protein size, buffer pH on protein-brush interactions and mimicked practical situation such as defect sites and long-term degradation. Strong chain length-dependent effects were already observed for PMP_{20}, PMP_{30}, and PMP_{50}, and we focus on data from these three chain lengths below.

Figure 4 shows the adsorbed mass density profiles obtained after HSA (1 g L^{-1}) and FIB solutions (0.15 g L^{-1}) in D_2O phosphate buffer were incubated over the PMP interface. Measurements were taken after incubation in protein solutions at neutral pH 7 for 1 h and then at pH 5 for another 1 h. The corresponding NR profiles are shown in Figure S2, and the best fit parameters are listed in Tables S3 and S4. The fitting analysis assumes that the underlying two-step distributions of the PMP chains shown in Figure 2B were preserved, but the thickness and density of each slice in the model were allowed to vary. Adsorbed proteins were modeled by either a single layer or two-step model as required for consistency with the NR data.

HSA incubation at pH 7 on PMP_{20} (Figure 4A) at the chain density chosen (0.22 nm^{-2}) led to the formation of a single overlayer of adsorbed mass with a thickness of 30 Å but a relatively low protein volume fraction (ϕ_{HSA}) of only 0.146, giving the adsorbed amount of Γ_{HSA} = 0.61 mg m^{-2} (Table S3). Compared to incubation at the corresponding pH on bare SiO_2/D_2O (Table S2), half of the adsorption was prevented. The single-step HSA model, in contrast to the two-step protein layer model required to describe adsorption on the SiO_2 control, also indicated the ability of PMP_{20} to limit surface-induced denaturation. Moreover, no changes to the PMP_{20} two-step layer structure was required to fit the data after protein adsorption-the HSA appeared to simply be associated with the top of the brush layer and not penetrating it.

As the chain length increased, the antifouling effect increased significantly, as expected from theories of brush behavior.[14,47] At the PMP_{30} interface, HSA adsorption at pH 7 reduced to Γ_{HSA} = 0.28 mg m^{-2} and it could be described by a single layer with an effective thickness of 25 Å and an even lower ϕ_{HSA} of 0.081 (Figure 4C), meaning that adsorption decreased by half compared to the PMP_{20} interface. Again, no changes to the PMP two-step layer structure was observed.

Reducing pH to 5 near HSA's IEP (4.8) increased adsorption, as expected. On PMP_{20}, Γ_{HSA} was 1.18 mg m^{-2} (Figure 4A). The amount adsorbed was now similar to that on the SiO_2 control, but a single step protein layer was sufficient to describe the data (i.e., no apparent protein spreading). The increased Γ_{HSA} meant that a denser HSA layer was formed (ϕ_{HSA} = 0.341), and it was also slightly thinner than the one at pH 7. Some protein structural deformation is implied by a fitted protein layer thickness (25 Å) that is much only around half of the shortest side of HSA (ca. 45 Å). On the other hand, still no changes to the two-step PMP_{20} layer structure was required to described the data.

With the slightly longer PMP_{30}, no compression of the protein layer was observed with a decrease to pH 5, although the amount of adsorption (Γ = 0.96 mg m^{-2} and ϕ_{HSA} = 0.276) was still higher than that at pH 7 (Figure 4C). However, with further increase in the chain length to PMP_{50} (accompanied by the lowest grafting density), an increased adsorption at pH 5 (Γ_{HSA} = 1.34 mg m^{-2}; thickness = 35 Å) caused a significant compression of the brush layer (Figure 4E). Our fitting still produced a single-step protein layer, but the PMP_{50} model showed a decreased inner slice height from 30 to 12 Å and an increased $\phi_{PMP\text{-}inner}$ from 0.258 to 0.751, while the upper "brush" slice also decreased in height from 35 to 12 Å and $\phi_{PMP\text{-}outer}$ increased from 0.079 to 0.123. This indicated a large redistribution of PMP_{50} chains down to the surface.

Analogous experiments were carried out using the much larger protein FIB (ca. 50 × 50 × 470 $Å^3$). As with HSA, lower adsorption was observed on PMPs than on the bare SiO_2 control, and the amount adsorbed at pH 7 decreased with increasing brush length (Figure 4B,D,F). For example, the highest adsorption at pH 7 on the shortest PMP_{20} chain length was Γ_{FIB} = 1.27 mg m^{-2} (Table S4), significantly lower than that on SiO_2 (2.4 mg m^{-2}; Table S2). Moreover, the two-step PMP layer structures were also preserved for all chain lengths after adsorption.

In contrast to the HSA results, only minor increases in FIB adsorption accompanied a reduction in the pH from 7 to 5 (closer to FIB's IEP = 4.3). For example, the adsorbed amount on PMP_{20} at pH 5 was Γ_{FIB} = 1.33 mg m^{-2} (Table S3), a 5% increase from pH 7. Moreover, a "reversed" two-step protein layer model with a less dense lower slice adjacent to the top of the polypeptoid was required to describe the FIBs adsorbed at pH 7 (Figure 4B and Table S4)-$\phi_{FIB\text{-}lower}$ = 0.16 in the lower 30 Å thick slice and $\phi_{FIB\text{-}upper}$ = 0.338 in the thinner but denser 12 Å upper slice. Obviously, NR layer profiles are approximate descriptions of surface bound layers. Nonetheless, unlike FIB adsorbed on bare SiO_2 (Table S2), the fact that the center of mass of adsorbed FIB was oriented away from the surface indicated that FIB did not spread on the PMP_{20} brush. The total protein layer thickness of 42 Å was similar to the short axis of FIB, indicating that FIB adsorbed sideways, consistent with atomic force microscopy (AFM) imaging.[47]

FIB adsorption became much reduced as the chain length increased, and a single-step model was sufficient to describe the protein adsorption. At the PMP_{30} interface (Figure 4D), an identical single-step 35 Å thick FIB layer (ϕ_{FIB} = 0.196 and Γ_{FIB} = 0.98 mg m^{-2}) could describe the adsorption at both pH 5 and 7 (Table S4). For PMP_{50}, single-step FIB layers of ϕ_{FIB} =

https://dx.doi.org/10.1021/acs.langmuir.0c02247
Langmuir 2020, 36, 12309−12318

0.053 and 30 to 40 Å thickness were observed (Figure 4F, Table S4).

AFM was also used to corroborate the (lack of) morphological changes with FIB adsorption on polypeptoid-coated Si/SiO_2 wafers. Examples of PMP_{30} (0.1 mM and pH 7) adsorbed onto an SiO_2 substrate (bare Si wafer) before and after FIB adsorption are shown in Figure 5. The surface of our wafers is extremely smooth with root mean square roughness under 0.5 nm. Grafting of PMP_{30} preserved the overall flat surface, illustrating also the uniformity of the coating. Upon FIB incubation, the roughness increased by only a small amount and no clear features of assembled/aggregated structures were apparent, consistent with the relatively small amount of FIB adsorption measured by NR (Figure 4D) and the significant antifouling effect of the PMP_{30} coating.

Figure 6 summarizes the effects of the polypeptoids with different chain lengths. FIB adsorption at both pH 7 and 5

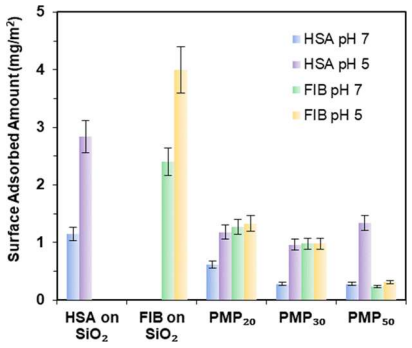

Figure 6. Summary of the antifouling effect of the PMP_n series of polypeptoids. Surface adsorbed amount of HSA and FIB on the silica surface (HSA/SiO_2 and FIB/SiO_2) as controls and on the preadsorbed polypeptoids surface at pH 7 and 5.

decreased with the chain length. Γ_{FIB} on PMP_{50} was roughly 3- and 4-folds lower than that on PMP_{30}, and PMP_{20}, respectively. Moreover, FIB adsorption on bare SiO_2, at 2.4 mg m^{-2} at pH 7 (Figure 6 and Table S2) and >4 mg m^{-2} at pH 5,[56] was considerably higher than that on all PMP surfaces. Thus, PMP interfaces were able to suppress FIB adsorption by 10−20 folds over the control even when the grafting densities were only around half of the "critical" values for preventing protein adsorption.

On the other hand, for HSA, Γ_{HSA} on PMP_{50} was reduced only by half at pH 7 when compared to the shortest PMP_{20}, and adsorption actually increased slightly at pH 5. In comparison, HSA adsorption on the bare SiO_2 control was 1.15 mg m^{-2} at pH 7 and 2.84 mg m^{-2} at pH 5 (Figure 6 and Table S2), which means that the current grafting densities only reduced adsorption of the smaller HSA by 3−4 folds.

The present results therefore emphasize that the superior antifouling performance of a longer brush (e.g. PMP_{50} vs PMP_{20}) is maintained for a protein that can be considered to be large relative to the spacing between grafted chains (at least in one dimension), even when the brush density is reduced. The large size of FIB also apparently rendered adsorption relatively insensitive to the effect of pH (i.e., electrostatic interactions). In contrast, resistance against adsorption of a smaller protein (e.g. HSA) was more readily compromised, especially for longer brushes which are more difficult to graft at higher surface densities. In particular, brush compression due to HSA adsorption was obvious on the least densely grafted PMP_{50} when the driving force for adsorption was high(er) (at pH 5-Figure 4E). Incidentally, the effectiveness of the present subcritical PMP_{50} surfaces is comparable to some PC polymer-coated surfaces.[3]

CONCLUSIONS

NR has enabled direct, *in situ* measurements of PMP polypeptoid layers, showing that they consisted of an inner dense region comprising adhesive DOPA pentapeptide and a sparse, highly hydrated, upper polymer brush region with a low volume fraction for all chain lengths and grafting densities studied. Buffer rinsing led to little removal of the bound polypeptoid, demonstrating a strong irreversibility in the surface interaction of the DOPA pentapeptide anchor on SiO_2, especially when the pentapeptide segment had sufficient space at lower grafting densities to spread on the surface.

NR also characterized in detail the PMP layer distributions and antifouling performances of the grafted PMPs. While our previous studies have already shown that PMP brushes could essentially eliminate protein adsorption at sufficiently high surface grafting densities,[47] we focused on lower PMP densities in the present experiments. This helped differentiate the effects of chain length, protein size, and environmental pH on adsorption and simulated practical antifouling challenges such as surface defects and brush degradation.

We found that polypeptoid surfaces were in fact more effective at reducing the adsorption of larger elongated FIB versus the smaller globular HSA, especially for longer chain lengths. This is similar to observations on zwitterionic PC-incorporated surfaces but different from classic model surfaces like flat SiO_2 and self-assembled monolayers such as octyldecyltrimethoxysilane (OTS) that obey the Vroman effect (higher affinity for larger proteins).[57,58] We also found that at a pH close to the protein's IEP, the resistance against adsorption of HSA decreased but it had little effect on adsorption of the larger FIB. Moreover, there was no indication of surface-induced denaturation on PMPs, which stands in contrast to the spreading and redistribution of protein mass toward the surface that we measured on the bare SiO_2 control (as well as generally observed on hydrophobic surfaces like OTS).

The contrast in antifouling behavior for PMPs compared to classic model surfaces indicates their strong repellent surface effect similar to observation on zwitterionic PC. However, our PMP is uncharged. AFM also revealed no structural feature characteristic of protein aggregation on PMPs, consistent with NR measurements. Although we show results for PMP only on SiO_2 (and previously on TiO_2),[17,47,59] excellent antifouling properties on various substrates have been demonstrated for polysarcosine,[60−62] a closely related antifouling peptoid, that we first reported with almost identical antifouling properties as PMP.[63] Therefore, peptoid coatings like PMP are very promising in applications such as preventing fouling on biomedical implants. In fact, our NR results also provide direct evidence of the extent to which a protein layer with relatively high adsorbed volume fraction (up to 0.3−0.7) can be supported on top of an underlying brush barrier layer with a much lower polymer fraction (<0.1) composed of mostly water. Even at the current subcritical brush densities, it appears that the adsorbed proteins were mostly interacting with the top of the PMP brushes, which suggests an opportunity to further improve antifouling if attractive protein−polymer interactions could be further reduced.

https://dx.doi.org/10.1021/acs.langmuir.0c02247
Langmuir 2020, 36, 12309−12318

■ ASSOCIATED CONTENT

Supporting Information

The Supporting Information is available free of charge at https://pubs.acs.org/doi/10.1021/acs.langmuir.0c02247.

NR profiles of HSA and FIB at SiO_2/D_2O buffer interfaces; NR profiles of HSA and FIB at PMP_n/D_2O buffer interfaces; molecular weights and SLDs of samples; best fitted parameters to the reflectivity data of HSA and FIB at SiO_2/D_2O buffer interfaces; best fitted parameters for HSA and FIB at PMP_n/D_2O buffer interfaces (PDF)

■ AUTHOR INFORMATION

Corresponding Authors

Jian R. Lu − *School of Physics & Astronomy, University of Manchester, Manchester M13 9PL, U.K.;* orcid.org/0000-0001-5648-3564; Email: J.Lu@manchester.ac.uk

Xiubo Zhao − *School of Pharmacy, Changzhou University, Changzhou 213164, China; Department of Chemical and Biological Engineering, University of Sheffield, Sheffield S1 3JD, U.K.;* orcid.org/0000-0002-4620-2893; Email: xiubo.zhao@sheffield.ac.uk

Authors

Fang Pan − *School of Pharmacy, Changzhou University, Changzhou 213164, China; School of Physics & Astronomy, University of Manchester, Manchester M13 9PL, U.K.*

King Hang Aaron Lau − *Department of Pure & Applied Chemistry, University of Strathclyde, Glasgow G1 1XL, U.K.;* orcid.org/0000-0003-3676-9228

Phillip B. Messersmith − *Department of Materials Science and Engineering, Department of Bioengineering, University of California−Berkeley, Berkeley, California 94720, United States;* orcid.org/0000-0002-1197-333X

Complete contact information is available at: https://pubs.acs.org/10.1021/acs.langmuir.0c02247

Notes

The authors declare no competing financial interest.

■ ACKNOWLEDGMENTS

We thank Engineering and Physical Sciences Research Council (EPSRC) for financial support under grants EP/F062966/1, EP/N007174/1, and EP/N023579/1, ISIS Neutron Facility at the Rutherford Appleton Laboratory for provision of neutron beam time and Jiangsu specially appointed professor program for support.

■ REFERENCES

(1) Nir, S.; Reches, M. Bio-inspired antifouling approaches: the quest towards non-toxic and non-biocidal materials. *Curr. Opin. Biotechnol.* **2016**, *39*, 48−55.

(2) Li, Z.; Pan, F.; Li, R.; Pambou, E.; Hu, X.; Ruane, S.; Ciumac, D.; Li, P.; Welbourn, R. J. L.; Webster, J. R. P.; Bishop, S. M.; Narwal, R.; van der Walle, C. F.; Lu, J. R. Coadsorption of a Monoclonal Antibody and Nonionic Surfactant at the SiO2/Water Interface. *ACS Appl. Mater. Interfaces* **2018**, *10*, 44257−44266.

(3) Murphy, E. F.; Lu, J. R.; Lewis, A. L.; Brewer, J.; Russell, J.; Stratford, P. Characterization of Protein Adsorption at the Phosphorylcholine Incorporated Polymer-Water Interface. *Macromolecules* **2000**, *33*, 4545−4554.

(4) Lu, J. R.; Murphy, E. F.; Su, T. J.; Lewis, A. L.; Stratford, P. W.; Satija, S. K. Reduced Protein Adsorption on the Surface of a Chemically Grafted Phospholipid Monolayer. *Langmuir* **2001**, *17*, 3382−3389.

(5) Damodaran, V. B.; Murthy, N. S. Bio-inspired strategies for designing antifouling biomaterials. *Biomater. Res.* **2016**, *20*, 18.

(6) Maan, A. M. C.; Hofman, A. H.; Vos, W. M.; Kamperman, M. Recent Developments and Practical Feasibility of Polymer-Based Antifouling Coatings. *Adv. Funct. Mater.* **2020**, *30*, 2000936.

(7) Zhao, X.; Pan, F.; Lu, J. R. Interfacial assembly of proteins and peptides: recent examples studied by neutron reflection. *J. R. Soc., Interface* **2009**, *6*, S659−S670.

(8) Ostuni, E.; Chapman, R. G.; Holmlin, R. E.; Takayama, S.; Whitesides, G. M. A survey of structure-property relationships of surfaces that resist the adsorption of protein. *Langmuir* **2001**, *17*, 5605−5620.

(9) Lu, J. R.; Su, T. J.; Thirtle, P. N.; Thomas, R. K.; Rennie, A. R.; Cubitt, R. The denaturation of lysozyme layers adsorbed at the hydrophobic solid/liquid surface studied by neutron reflection. *J. Colloid Interface Sci.* **1998**, *206*, 212−223.

(10) Su, T. J.; Lu, J. R.; Thomas, R. K.; Cui, Z. F. Effect of pH on the Adsorption of Bovine Serum Albumin at the Silica/Water Interface Studied by Neutron Reflection. *J. Phys. Chem. B* **1999**, *103*, 3727−3736.

(11) Su, T. J.; Lu, J. R.; Thomas, R. K.; Cui, Z. F.; Penfold, J. The Conformational Structure of Bovine Serum Albumin Layers Adsorbed at the Silica-Water Interface. *J. Phys. Chem. B* **1998**, *102*, 8100−8108.

(12) Su, T. J.; Lu, J. R.; Thomas, R. K.; Cui, Z. F.; Penfold, J. The effect of pH on the adsorption of lysozyme at the hydrophilic silicon oxide-water interface, a neutron reflection study. *Langmuir* **1998**, *14*, 438−445.

(13) Attwood, S. J.; Kershaw, R.; Uddin, S.; Bishop, S. M.; Welland, M. E. Understanding how charge and hydrophobicity influence globular protein adsorption to alkanethiol and material surfaces. *J. Mater. Chem. B* **2019**, *7*, 2349−2361.

(14) Satulovsky, J.; Carignano, M. A.; Szleifer, I. Kinetic and thermodynamic control of protein adsorption. *Proc. Natl. Acad. Sci. U.S.A.* **2000**, *97*, 9037−9041.

(15) Yang, L.; Pan, F.; Zhao, X.; Yaseen, M.; Padia, F.; Coffey, P.; Freund, A.; Yang, L.; Liu, T.; Ma, X.; Lu, J. R. Thermoresponsive copolymer nanofilms for controlling cell adhesion, growth, and detachment. *Langmuir* **2010**, *26*, 17304−17314.

(16) Statz, A. R.; Kuang, J.; Ren, C.; Barron, A. E.; Szleifer, I.; Messersmith, P. B. Experimental and theoretical investigation of chain length and surface coverage on fouling of surface grafted polypeptoids. *Biointerphases* **2009**, *4*, FA22−FA32.

(17) Statz, A. R.; Meagher, R. J.; Barron, A. E.; Messersmith, P. B. New Peptidomimetic Polymers for Antifouling Surfaces. *J. Am. Chem. Soc.* **2005**, *127*, 7972−7973.

(18) Lau, K. H. A.; Sileika, T. S.; Park, S. H.; Sousa, A. M. L.; Burch, P.; Szleifer, I.; Messersmith, P. B. Molecular Design of Antifouling Polymer Brushes Using Sequence-Specific Peptoids. *Adv. Mater. Interfaces* **2015**, *2*, 1400225.

(19) Lau, K. H. A. Peptoids for biomaterials science. *Biomater. Sci.* **2014**, *2*, 627−633.

(20) Lu, J. R. Neutron reflection study of globular protein adsorption at planar interfaces. *Annu. Rep. Prog. Chem., Sect. C: Phys. Chem.* **1999**, *95*, 3−46.

(21) Lu, J. R.; Perumal, S.; Powers, E. T.; Kelly, J. W.; Webster, J. R. P.; Penfold, J. Adsorption of β-Hairpin Peptides on the Surface of Water: A Neutron Reflection Study. *J. Am. Chem. Soc.* **2003**, *125*, 3751−3757.

(22) Lu, J. R.; Perumal, S.; Hopkinson, I.; Webster, J. R. P.; Penfold, J.; Hwang, W.; Zhang, S. Interfacial Nano-structuring of Designed Peptides Regulated by Solution pH. *J. Am. Chem. Soc.* **2004**, *126*, 8940−8947.

(23) Lu, J. R.; Su, T.-J.; Georganopoulou, D.; Williams, D. E. Interfacial dissociation and unfolding of glucose oxidase. *J. Phys. Chem. B* **2003**, *107*, 3954−3962.

(24) Lu, J.; Zhao, X.; Yaseen, M. Protein Adsorption Studied by Neutron Reflection. *Curr. Opin. Colloid Interface Sci.* **2007**, *12*, 9−16.

(25) Jayawardane, D.; Pan, F.; Lu, J. R.; Zhao, X. Co-adsorption of peptide amphiphile V(6)K and conventional surfactants SDS and C(12)TAB at the solid/water interface. *Soft Matter* **2015**, *11*, 7986−7994.
(26) Jayawardane, D.; Pan, F.; Lu, J. R.; Zhao, X. Interfacial Adsorption of Silk Fibroin Peptides and Their Interaction with Surfactants at the Solid-Water Interface. *Langmuir* **2016**, *32*, 8202−8211.
(27) Pan, F.; Li, Z.; Gong, H.; Petkov, J. T.; Lu, J. R. Membrane-lytic actions of sulphonated methyl ester surfactants and implications to bactericidal effect and cytotoxicity. *J. Colloid Interface Sci.* **2018**, *531*, 18−27.
(28) Wang, J.; Jia, D.; Tao, K.; Wang, C.; Zhao, X.; Yaseen, M.; Xu, H.; Que, G.; Webster, J. R. P.; Lu, J. R. Interfacial assembly of lipopeptide surfactants on octyltrimethoxysilane-modified silica surface. *Soft Matter* **2013**, *9*, 9684−9691.
(29) Jia, D.; Tao, K.; Wang, J.; Wang, C.; Zhao, X.; Yaseen, M.; Xu, H.; Que, G.; Webster, J. R. P.; Lu, J. R. Interfacial adsorption of lipopeptide surfactants at the silica/water interface studied by neutron reflection. *Soft Matter* **2011**, *7*, 1777−1788.
(30) Jia, D.; Tao, K.; Wang, J.; Wang, C.; Zhao, X.; Yaseen, M.; Xu, H.; Que, G.; Webster, J. R. P.; Lu, J. R. Dynamic adsorption and structure of interfacial bilayers adsorbed from lipopeptide surfactants at the hydrophilic silicon/water interface: effect of head group length. *Langmuir* **2011**, *27*, 8798−8809.
(31) Zhao, X.; Pan, F.; Perumal, S.; Xu, H.; Lu, J. R.; Webster, J. R. P. Interfacial Assembly of Cationic Peptide Surfactants. *Soft Matter* **2009**, *5*, 1630−1638.
(32) Pan, F.; Zhao, X.; Perumal, S.; Waigh, T. A.; Lu, J. R.; Webster, J. R. P. Interfacial Dynamic Adsorption and Structure of Molecular Layers of Peptide Surfactants. *Langmuir* **2010**, *26*, 5690−5696.
(33) Pan, F.; Zhao, X.; waigh, T. A.; Lu, J. R.; Miano, F. Interfacial adsorption and denaturization of human milk and recombinant rice lactoferrin. *Biointerphases* **2008**, *3*, FB36−FB43.
(34) Xu, H.; Zhao, X.; Grant, C.; Lu, J. R.; Williams, D. E.; Penfold, J. Orientation of a Monoclonal Antibody Adsorbed at the Solid/Solution Interface: A Combined Study Using Atomic Force Microscopy and Neutron Reflectivity. *Langmuir* **2006**, *22*, 6313−6320.
(35) Xu, H.; Perumal, S.; Zhao, X.; Du, N.; Liu, X.-Y.; Jia, Z.; Lu, J. R. Interfacial Adsorption of Antifreeze Proteins: a neutron reflection study. *Biophys. J.* **2008**, *94*, 4405−4413.
(36) Miano, F.; Zhao, X.; Lu, J. R.; Penfold, J. Coadsorption of Human Milk Lactoferrin into the Dipalmitoylglycerolphosphatidylcholine Phospholipid Monolayer Spread at the Air/Water Interface. *Biophys. J.* **2007**, *92*, 1254−1262.
(37) Lu, J. R.; Perumal, S.; Zhao, X.; Miano, F.; Enea, V.; Heenan, R. R.; Penfold, J. Surface-induced unfolding of human lactoferrin. *Langmuir* **2005**, *21*, 3354−3361.
(38) Pan, F.; Li, Z.; Leyshon, T.; Rouse, D.; Li, R.; Smith, C.; Campana, M.; Webster, J. R. P.; Bishop, S. M.; Narwal, R.; van der Walle, C. F.; Warwicker, J.; Lu, J. R. Interfacial Adsorption of Monoclonal Antibody COE-3 at the Solid/Water Interface. *ACS Appl. Mater. Interfaces* **2018**, *10*, 1306−1316.
(39) Li, Z.; Li, R.; Smith, C.; Pan, F.; Campana, M.; Webster, J. R. P.; van der Walle, C. F.; Uddin, S.; Bishop, S. M.; Narwal, R.; Warwicker, J.; Lu, J. R. Neutron Reflection Study of Surface Adsorption of Fc, Fab, and the Whole mAb. *ACS Appl. Mater. Interfaces* **2017**, *9*, 23202−23211.
(40) Smith, C.; Li, Z.; Holman, R.; Pan, F.; Campbell, R. A.; Campana, M.; Li, P.; Webster, J. R. P.; Bishop, S.; Narwal, R.; Uddin, S.; van der Walle, C. F.; Lu, J. R. Antibody adsorption on the surface of water studied by neutron reflection. *mAbs* **2017**, *9*, 466−475.
(41) Zhao, X.; Pan, F.; Cowsill, B.; Lu, J. R.; Garcia-Gancedo, L.; Flewitt, A. J.; Ashley, G. M.; Luo, J. Interfacial Immobilization of Monoclonal Antibody and Detection of Human Prostate-Specific Antigen. *Langmuir* **2011**, *27*, 7654−7662.
(42) Zhao, X.; Pan, F.; Garcia-Gancedo, L.; Flewitt, A. J.; Ashley, G. M.; Luo, J.; Lu, J. R. Interfacial Recognition of Human Prostate-Specific Antigen by Immobilized Monoclonal Antibody: Effects of Solution Conditions and Surface Chemistry. *J. R. Soc., Interface* **2012**, *9*, 2457−2467.
(43) Cowsill, B. J.; Zhao, X.; Waigh, T. A.; Eapen, S.; Davies, R.; Laux, V.; Haertlein, M.; Forsyth, V. T.; Lu, J. R. Interfacial structure of immobilized antibodies and perdeuterated HSA in model pregnancy tests measured with neutron reflectivity. *Langmuir* **2014**, *30*, 5880−5887.
(44) Zhao, X.; Pan, F.; Coffey, P.; Lu, J. R. Cationic Copolymer-Mediated DNA Immobilization: Interfacial Structure and Composition As Determined by Ellipsometry, Dual Polarization Interferometry, and Neutron Reflection. *Langmuir* **2008**, *24*, 13556−13564.
(45) Zhang, J.; Taylor, D. J. F.; Li, P. X.; Thomas, R. K.; Wang, J. B.; Penfold, J. Adsorption of DNA and Dodecyl Trimethylammonium Bromide Mixtures at the Air/Water Interface: A Neutron Reflectometry Study. *Langmuir* **2008**, *24*, 1863−1872.
(46) Hughes, A. V.; Goldar, A.; Gerstenberg, M. C.; Roser, S. J.; Bradshaw, J. A hybrid SAM phospholipid approach to fabricating a "free"supported lipid bilayer. *Phys. Chem. Chem. Phys.* **2002**, *4*, 2371−2378.
(47) Lau, K. H. A.; Ren, C.; Park, S. H.; Szleifer, I.; Messersmith, P. B. An experimental-theoretical analysis of protein adsorption on peptidomimetic polymer brushes. *Langmuir* **2012**, *28*, 2288−2298.
(48) Knight, A. S.; Zhou, E. Y.; Francis, M. B.; Zuckermann, R. N. Sequence Programmable Peptoid Polymers for Diverse Materials Applications. *Adv. Mater.* **2015**, *27*, 5665−5691.
(49) Cheng, W.; Zeng, X.; Chen, H.; Li, Z.; Zeng, W.; Mei, L.; Zhao, Y. Versatile Polydopamine Platforms: Synthesis and Promising Applications for Surface Modification and Advanced Nanomedicine. *ACS Nano* **2019**, *13*, 8537−8565.
(50) Lu, J. R.; Lee, E. M.; Thomas, R. K. The Analysis and Interpretation of Neutron and X-ray Specular Reflection. *Acta Crystallogr., Sect. A: Cryst. Phys., Diffr., Theor. Gen. Crystallogr.* **1996**, *52*, 11−41.
(51) Cheung, D. L.; Lau, K. H. A. Atomistic Study of Zwitterionic Peptoid Antifouling Brushes. *Langmuir* **2019**, *35*, 1483−1494.
(52) Ghuman, J.; Zunszain, P. A.; Petitpas, I.; Bhattacharya, A. A.; Otagiri, M.; Curry, S. Structural basis of the drug-binding specificity of human serum albumin. *J. Mol. Biol.* **2005**, *353*, 38−52.
(53) Yaseen, M.; Zhao, X.; Freund, A.; Seifalian, A. M.; Lu, J. R. Surface Structural Conformations Of Fibrinogen Polypeptides For Improved Biocompatibility. *Biomaterials* **2010**, *31*, 3781−3792.
(54) Lau, K. H. A.; Tan, L.-S.; Tamada, K.; Sander, M. S.; Knoll, W. Highly sensitive detection of processes occurring inside nanoporous anodic alumina templates: A waveguide optical study. *J. Phys. Chem. B* **2004**, *108*, 10812−10818.
(55) Talbot, J.; Tarjus, G.; Van Tassel, P. R.; Viot, P. From car parking to protein adsorption: an overview of sequential adsorption processes. *Colloids Surf., A* **2000**, *165*, 287−324.
(56) Yaseen, M.; Salacinski, H. J.; Seifalian, A. M.; Lu, J. R. Dynamic protein adsorption at the polyurethane copolymer/water interface. *Biomed. Mater.* **2008**, *3*, 034123.
(57) Vroman, L. Effect of Adsorbed Proteins on the Wettability of Hydrophilic and Hydrophobic Solids. *Nature* **1962**, *196*, 476−477.
(58) Unsworth, L. D.; Sheardown, H.; Brash, J. L. Polyethylene oxide surfaces of variable chain density by chemisorption of PEO-thiol on gold: adsorption of proteins from plasma studied by radiolabelling and immunoblotting. *Biomaterials* **2005**, *26*, 5927−5933.
(59) Statz, A. R.; Barron, A. E.; Messersmith, P. B. Protein, cell and bacterial fouling resistance of polypeptoid-modified surfaces: effect of side-chain chemistry. *Soft Matter* **2008**, *4*, 131−139.
(60) Gao, Q.; Li, P.; Zhao, H.; Chen, Y.; Jiang, L.; Ma, P. X. Methacrylate-ended polypeptides and polypeptoids for antimicrobial and antifouling coatings. *Polym. Chem.* **2017**, *8*, 6386−6397.
(61) Schneider, M.; Tang, Z.; Richter, M.; Marschelke, C.; Förster, P.; Wegener, E.; Amin, I.; Zimmermann, H.; Scharnweber, D.; Braun, H.-G.; Luxenhofer, R.; Jordan, R. Patterned Polypeptoid Brushes. *Macromol. Biosci.* **2016**, *16*, 75−81.

https://dx.doi.org/10.1021/acs.langmuir.0c02247
Langmuir 2020, 36, 12309−12318

(62) Bleher, S.; Buck, J.; Muhl, C.; Sieber, S.; Barnert, S.; Witzigmann, D.; Huwyler, J.; Barz, M.; Suss, R. Poly(Sarcosine) Surface Modification Imparts Stealth-Like Properties to Liposomes. *Small* **2019**, *15*, 1904716.
(63) Lau, K. H. A.; Ren, C.; Sileika, T. S.; Park, S. H.; Szleifer, I.; Messersmith, P. B. Surface-grafted polysarcosine as a peptoid antifouling polymer brush. *Langmuir* **2012**, *28*, 16099−16107.

https://dx.doi.org/10.1021/acs.langmuir.0c02247
Langmuir 2020, 36, 12309−12318